ARTICLE

Hybrid Multi-Infeed Interaction Factor Calculation Method Considering Voltage Regulation Control Characteristics of Voltage Source Converter

Shan Liu[1], Chengbin Chi[1], Fengze Han[2], Yanan Wu[1], Lin Zhu[1] and Tuo Wang[2,*]

[1]State Grid Smart Grid Research Institute, State Grid Corporation of China, Beijing, 102209, China

[2]School of Electric Power Engineering, Northeast Electric Power University, Jilin, 132012, China

[*]Corresponding Author: Tuo Wang. Email: wangtuo950408@163.com

ABSTRACT

Voltage source converter based high voltage direct current (VSC-HVDC) can participate in voltage regulation by flexible control to help maintain the voltage stability of the power grid. In order to quantitatively evaluate its influence on the voltage interaction between VSC-HVDC and line commutated converter based high voltage direct current (LCC-HVDC), this paper proposes a hybrid multi-infeed interaction factor (HMIIF) calculation method considering the voltage regulation control characteristics of VSC-HVDC. Firstly, for a hybrid multi-infeed high voltage direct current system, an additional equivalent operating admittance matrix is constructed to characterize HVDC equipment characteristics under small disturbance. Secondly, based on the characteristic curve between the reactive power and the voltage of a certain VSC-HVDC project, the additional equivalent operating admittance of VSC-HVDC is derived. The additional equivalent operating admittance matrix calculation method is proposed. Thirdly, the equivalent bus impedance matrix is obtained by modifying the alternating current (AC) system admittance matrix with the additional equivalent operating admittance matrix. On this basis, the HMIIF calculation method based on the equivalent bus impedance ratio is proposed. Finally, the effectiveness of the proposed method is verified in a hybrid dual-infeed high voltage direct current system constructed in Power Systems Computer Aided Design (PSCAD), and the influence of voltage regulation control on HMIIF is analyzed.

KEYWORDS

Hybrid multi-infeed high voltage direct current system; hybrid multi-infeed interaction factor; control modes; equivalent node impedance ratio; voltage interaction characteristics

1 Introduction

The line commutated converter based high voltage direct current (LCC-HVDC) is widely used in large-capacity and long-distance transmission occasions [1,2]. Multi-infeed high voltage direct current system (MIDC) is formed by several LCC-HVDC links with close electrical distance and the receiving-end alternating current (AC) power grid. There is a strong interaction among inverters, which greatly affects the static and dynamic characteristics of the receiving-end AC power grid [3,4]. Compared with LCC-HVDC, voltage source converter based high voltage direct current (VSC-HVDC) has a more flexible control performance and can participate in voltage regulation to help to maintain the voltage stability of the power grid [5–7]. With the construction of VSC-HVDC projects, the situation

gradually increases that VSC-HVDC is fed into the original MIDC system, and then a hybrid multi-infeed high voltage direct current system (HMIDC) is formed. The receiving-end power grid will show new operating characteristics due to the complex interactions among multiple inverters of different types [8–10]. The research on the interaction of multiple inverters in MIDC and HMIDC is of great significance for the planning and operation of the receiving-end power grid.

To evaluate the voltage interaction between the inverters in the MIDC, the CIGRE working group proposed the index of multi-infeed interaction factor (MIIF) [11]. MIIF is an experimental index by definition, which needs to be obtained through multiple simulations. For complex large-scale power grids, it cannot adapt to the changes in the structure and operation mode of the power grid, and it takes a lot of time for simulation. Due to the deficiencies of the simulation method, the fast calculation method of MIIF based on the impedance ratio is adopted [12–14]. The method only needs to form the AC system impedance matrix to calculate MIIF. However, the influence of the control response characteristics of LCC-HVDC is ignored in the method. Considering the control response characteristics of LCC-HVDC, the power flow equation is modified by the sensitivity of active and reactive power delivered from inverters to the bus voltage, and the calculation method of MIIF based on the Jacobian matrix is proposed [15]. Although the method has a clear physical meaning, it cannot consider the dynamic impedance characteristics of the power source, load, and other components. To take the dynamic impedance characteristics of power equipment into account, an improvement method of the equivalent impedance ratio is proposed, and the influence of the active power delivered from the inverters on the bus voltage is neglected in the method [16]. Considering the influence of active and reactive power on inverter bus voltage, the MIIF calculation method under small disturbance is proposed [17].

In the HMIDC, there are some great research efforts on the interaction of multiple inverters. The positive contribution of the VSC-HVDC link to the LCC-HVDC link in the area of commutation failure immunity index, effective short circuit ratio, voltage sensitivity factor, temporary overvoltage, and DC line fault recovery are investigated [18]. The methods of analyzing and evaluating the interaction between VSC-HVDC and LCC-HVDC control systems are proposed [19,20]. The MIIF calculation method of the HMIDC considering DC control response characteristics is proposed [21]. Few studies focus on the MIIF of the HMIDC, though it is valuable for evaluating the voltage and power stability, the risk of LCC-HVDC commutation failure, and the interaction of harmonics [22–24]. In projects, VSC-HVDC can be equipped with voltage regulation control to enhance voltage stability, which affects the voltage interaction between the inverters. It is necessary to study the MIIF calculation method in HMIDC considering the voltage regulation control characteristics of VSC-HVDC. The following two problems need to be solved:

1) How to calculate MIIF quickly and accurately in the HMIDC system.

2) How to consider the voltage regulation characteristics of VSC-HVDC during the fast calculation of MIIF.

Facing these issues, the following contributions are made:

1) Referring to the MIIF of the MIDC system, the hybrid multi-infeed interaction factor (HMIIF) of the HMIDC system is defined to describe the voltage interaction between VSC-HVDC and LCC-HVDC. The HMIIF calculation method based on the equivalent bus impedance ratio is proposed. The equivalent bus impedance matrix is obtained by modifying the AC system admittance matrix with the additional equivalent operating admittance matrix considering the characteristics of HVDC. HMIIF is calculated based on the equivalent bus impedance ratio.

2) Based on the voltage regulation control characteristic curve of a certain VSC-HVDC project, the additional equivalent operating admittance under the control of VSC-HVDC is derived to reflect the control characteristics. Under the voltage regulation control, the admittance is updated and used in the HMIIF calculation method based on the equivalent bus impedance ratio.

This paper proposes the HMIIF calculation method considering voltage regulation control characteristics of VSC-HVDC. Based on the power system network equations, the additional equivalent operating admittance matrix considering the control response characteristics of DC under small disturbance is established. According to the characteristic curve between the reactive power and the voltage of a certain VSC-HVDC project, the additional equivalent operating admittances are derived, and the additional equivalent operating admittance matrix is constructed. The AC system impedance matrix is modified by the additional equivalent operating admittance matrix, and the equivalent bus impedance matrix is obtained. The HMIIF is calculated by the equivalent bus impedance ratio. The simulation model of the hybrid dual-infeed DC system is built in PSCAD/EMTDC to verify that the calculation method can effectively obtain the index HMIIF.

2 Impedance Modeling of HMIDC

In the MIDC, MIIF can be used to evaluate the voltage interaction between the inverters. Similarly, to describe the voltage interaction between the inverters in the HMIDC, the hybrid multi-feed interaction factor (HMIIF) can be introduced. HMIIF_{ji} is the ratio of the voltage changes at the inverter buses j and i in HMIDC when inverter bus i induces an approximate 1% step voltage through the artificial switched connection of a shunt reactive element.

$$\text{HMIIF}_{ji} = \frac{\Delta U_j}{\Delta U_i} = \frac{\Delta U_j}{1\% U_i} \tag{1}$$

where ΔU_i and ΔU_j are the voltage change rate of the inverter bus i and j, and U_i is the voltage of the inverter bus i before the voltage step.

Assuming a total of N inverters are connected to the receiving-end power grid, there are k LCC-HVDC links and N-k VSC-HVDC links. Based on the multi-port Thevenin equivalent method, a simplified model of the HMIDC can be established, as shown in Fig. 1. In the figure, $E_i \angle \xi_i$ and Z_i are the AC equivalent source voltage and impedance of inverter i, K_i and $X_{\text{T}i}$ are the transformation ratio and leakage reactance of the transformer connected to inverter i, $U_i \angle \theta_i$ and B_{ci} are the equivalent admittance of bus voltage and reactive power compensation capacitor of inverter i, and $Z_{i,j}$ is the equivalent coupling impedance between inverter i and j.

According to the power network equation, the bus voltage U_j of the inverter j before the voltage step can be expressed as:
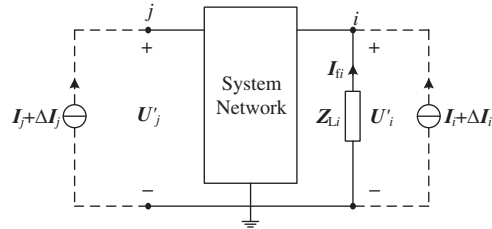
$$U_j = \sum_{m=1}^{N} Z_{jm} I_m \tag{2}$$

where Z_{jm} is the mutual impedance between the bus nodes of inverter j and m, and I_m is the current injected into the bus node of the inverter m.

According to the definition of HMIIF, it is assumed that the shunt reactor $Z_{\text{L}i}$ is connected to the bus of inverter i, which induces an approximate 1% step voltage. The equivalent circuit of the system after the voltage step is shown in Fig. 2.
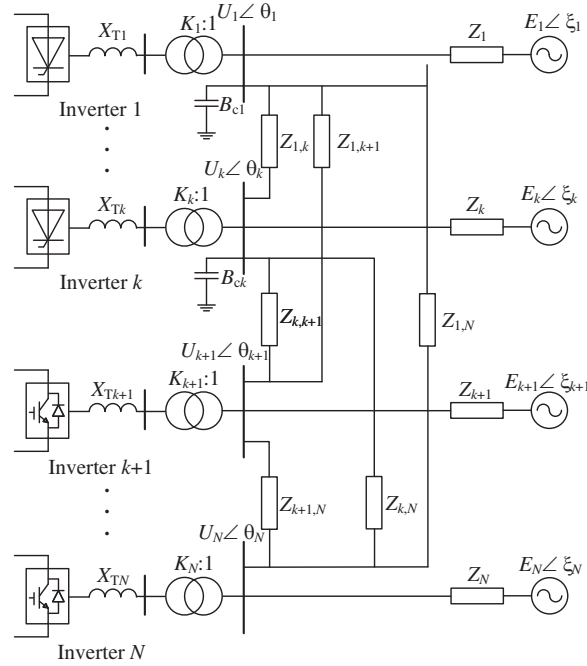
Figure 1: Simplified HMIDC system model

Figure 2: Equivalent circuit after voltage step

After the voltage step, the bus voltage U'_j of inverter j can be written as:

$$U'_j = \sum_{m=1}^{N} \boldsymbol{Z}_{jm} \left(\boldsymbol{I}_m + \Delta \boldsymbol{I}_m \right) + \boldsymbol{Z}_{ji} \boldsymbol{I}_{fi} \tag{3}$$

where $\boldsymbol{I}_{fi}$ is the current flowing from the grounding point to the bus node of the inverter i through the reactor $\boldsymbol{Z}_{Li}$, and $\Delta \boldsymbol{I}_m$ is the current variation caused by the voltage step.

The bus voltage U'_i of inverter i can be expressed as:

$$\begin{cases} U'_i = \sum\limits_{m=1}^{N} \boldsymbol{Z}_{im} \left(\boldsymbol{I}_m + \Delta \boldsymbol{I}_m \right) + \boldsymbol{Z}_{ii} \boldsymbol{I}_{fi} \\ U'_i = -\boldsymbol{Z}_{Li} \boldsymbol{I}_{fi} \end{cases} \tag{4}$$

By calculating (4), the current $I_{\mathrm{f}i}$ can be obtained as:

$$I_{\mathrm{f}i} = -\frac{1}{Z_{ii} + Z_{\mathrm{L}i}} \sum_{m=1}^{N} Z_{im} (I_m + \Delta I_m) \tag{5}$$

The voltage variation ΔU_j can be further written as:

$$\Delta U_j = U_j' - U_j = \sum_{m=1}^{N} Z_{jm} \Delta I_m + \frac{Z_{ji}}{Z_{ii} + Z_{\mathrm{L}i}} \sum_{m=1}^{N} Z_{im} (I_m + \Delta I_m) \tag{6}$$

If rewriting (6) into the vector, the expression can be given:

$$\Delta U_j - Z_{ji} I_{\mathrm{f}i} - Z_{j0} \cdot \Delta I = 0 \tag{7}$$

where Z_{j0} is the row vector composed of the jth row elements of the AC system impedance matrix Z, and ΔI is the column vector of the current variation.

If rewriting (7) into the matrix, the following expression can be given:

$$\Delta U - Z_{0i} I_{\mathrm{f}i} - Z \cdot \Delta I = 0 \tag{8}$$

where Z_{0i} is a column vector composed of elements in the ith column of the AC system impedance matrix Z, and ΔU is the column vector of the voltage variation.

In the case of small disturbances, it can be considered that the power grid is linear near the steady-state operating point, and the additional equivalent operating admittance at the bus node of inverter m is defined as:

$$Y_{\Delta m} = \frac{\Delta I_m}{\Delta U_m} \tag{9}$$

The matrix Y_Δ with the additional equivalent operating admittance as the main diagonal elements can be constructed. Rewriting (9) into the matrix, the expression can be given:

$$\Delta I = Y_\Delta \cdot \Delta U \tag{10}$$

By substituting (10) into (8), the column vector of the voltage variation can be deduced as:

$$\Delta U = (Y - Y_\Delta)^{-1} Y Z_{0i} I_{\mathrm{f}i} = (Y - Y_\Delta)^{-1} E_{0i} I_{\mathrm{f}i} \tag{11}$$

where E_{0i} is a column vector composed of elements in the ith column of the unit matrix E.

Assuming $Z_{\mathrm{eq}} = (Y - Y_\Delta)^{-1}$, (11) can be rewritten as:

$$\Delta U = Z_{\mathrm{eq}0i} I_{\mathrm{f}i} \tag{12}$$

Observing (12), it can be seen that under small disturbance, the voltage variation vector can be expressed as the product of the ith column vector of the equivalent bus impedance matrix and the current injected into the bus node of the inverter i by the shunt reactor $Z_{\mathrm{L}i}$.

3 Calculation of Additional Equivalent Operating Admittance

The additional equivalent operating admittance matrix is a diagonal matrix composed of additional equivalent operating admittance as its elements. The diagonal matrix elements need to be deduced.

For any inverter, the apparent power delivered by the inverter is $\boldsymbol{S}_I = \boldsymbol{U}_I \boldsymbol{I}_I^*$. Where $\boldsymbol{U}_I$ is the bus voltage of the inverter, and $\boldsymbol{I}_I$ is the current flowing from the inverter to the bus. Under small disturbances, apparent power variation $\Delta \boldsymbol{S}_I$ satisfy can be expressed as:

$$\Delta \boldsymbol{S}_I = (\boldsymbol{U}_I + \Delta \boldsymbol{U}_I)(\boldsymbol{I}_I + \Delta \boldsymbol{I}_I)^* - \boldsymbol{U}_I \boldsymbol{I}_I^* \tag{13}$$

Then, (13) can be written as:

$$\frac{\Delta \boldsymbol{I}_I^*}{\Delta \boldsymbol{U}_I^*} = \frac{\Delta \boldsymbol{S}_I}{(\boldsymbol{U}_I + \Delta \boldsymbol{U}_I)\,\Delta \boldsymbol{U}_I^*} - \frac{\Delta \boldsymbol{U}_I \boldsymbol{S}_I}{(\boldsymbol{U}_I + \Delta \boldsymbol{U}_I)\,\boldsymbol{U}_I \Delta \boldsymbol{U}_I^*} \tag{14}$$

According to the definition of HMIIF, the reactance of the shunt reactive element needs to be extremely large to show an approximate 1% step voltage in the bus. Before and after the voltage step, the variation of the phase angle of the bus voltage can be approximately ignored. Therefore, $\Delta \boldsymbol{U}_I = \varepsilon \boldsymbol{U}_I \, (0 < \varepsilon \ll 1)$ can be assumed, and ε is a real number. Furtherly, (14) can be written as:

$$\boldsymbol{Y}_{\Delta m} = \frac{\Delta \boldsymbol{I}_I}{\Delta \boldsymbol{U}_I} \approx \frac{1}{1+\varepsilon} \left(\frac{\Delta \boldsymbol{S}_I^*}{\boldsymbol{U}_I \cdot \Delta \boldsymbol{U}_I} - \frac{\boldsymbol{S}_I^*}{U_I^2} \right) \approx \frac{\Delta \boldsymbol{S}_I^*}{\boldsymbol{U}_I \cdot \Delta \boldsymbol{U}_I} - \frac{\boldsymbol{S}_I^*}{U_I^2} \tag{15}$$

Under the steady-state operation of the HMIDC, the system operating parameters can be known. If the functional relationship between the apparent power and the magnitude of bus voltage is constructed and substituted into (15), the elements of the additional equivalent operating admittance matrix $\boldsymbol{Y}_\Delta$ can be calculated.

3.1 Equivalent Operating Admittance of LCC-HVDC

In the LCC-HVDC link, constant DC current (CC) control is used in the rectifier, while constant extinction angle (CE) control is used in the inverter. LCC-HVDC link satisfies the following operating equation:

$$P_I = U_{dI} I_d \tag{16}$$

$$Q_I = -P_I \tan \varphi_I \tag{17}$$

$$\boldsymbol{S}_I = P_I + j Q_I \tag{18}$$

$$U_{dI} = \frac{3\sqrt{2}}{\pi} K_I U_I \cos \gamma_I - \frac{3}{\pi} X_{TI} I_d \tag{19}$$

$$\cos \varphi_I = \cos \gamma_I - \frac{X_{TI} I_d}{\sqrt{2} K_I U_I} \tag{20}$$

where U_{dI} is the DC voltages of the inverter, P_I is the active power transmitted by the inverter, Q_I is the reactive power delivered by the inverter, K_I and X_{TI} are the transformation ratio and leakage reactance of the transformer connected to the inverter, φ_I and γ_I are the power factor angle and extinction angle of the inverter, respectively, and I_d is the DC current.

The functional relationship between the apparent power and the magnitude of the bus voltage for the LCC-HVDC link can be derived based on (16)–(20), and the additional equivalent operating admittances can be obtained [17]. Eq. (21) is the calculation equation for the additional equivalent

operating admittance for the LCC-HVDC link.

$$Y_{\Delta m} = \frac{3N_I X_{TI} I_d^2}{\pi U_I^2}\left(1 - j\frac{A}{\sqrt{2K_I^2 U_I^2 - A^2}}\right) \tag{21}$$

The relevant parameters A is followed as:

$$A = \sqrt{2}U_I K_I \cos\gamma_I - X_{TI} I_d \tag{22}$$

The additional equivalent operating admittance of the LCC-HVDC can be calculated based on the above equations.

3.2 Equivalent Operating Admittance of VSC-HVDC

For the VSC-HVDC link, the rectifier or the inverter needs to adopt CV control to keep the DC voltage constant while the other can adopt CP control. VSC-HVDC can be equipped with voltage regulation control to help to maintain the voltage stability of the AC grid in projects. Since the DC link can only transmit active power, there is no need to consider the voltage regulation control of the rectifier.

For a certain VSC-HVDC project with voltage regulation control in southern China, the characteristic curve between the reactive power and the bus voltage is shown in Fig. 3. When the bus voltage of the inverter is in the range of $[U_{low}, U_{high}]$, the inverter adopts constant reactive power (CQ) control. If the voltage is located in the range of $[U_{min}, U_{low}]$ or $[U_{high}, U_{max}]$, the voltage regulation control will be adopted. Assuming a large disturbance makes the voltage out of $[U_{min}, U_{max}]$, the ride-through control will be started. This paper focuses on the calculation of HMIIF under the small disturbance and analyzes the CQ control and the voltage regulation control rather than the ride-through control. In the project, $Q_{min} = -0.2$ pu, $Q_{max} = 0.2$ pu, $U_{min} = 0.9$ pu, $U_{max} = 1.1$ pu, $U_{low} = 0.95$ pu, and $U_{high} = 1.05$ pu.
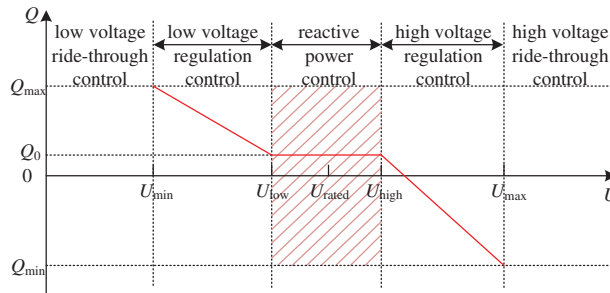
Figure 3: Characteristic curve between reactive power and bus voltage of a certain VSC-HVDC project

3.2.1 Constant Reactive Power (CQ) Control

In this control mode, the reactive power Q_I delivered by the inverter is constant Q_0. While the rectifier adopts constant active power (CP) control and active power transmitted is P_R, the inverter adopts constant DC voltage (CV) control and DC voltage is U_{dI}. The steady-state equation of VSC-HVDC can be expressed as:

$$\begin{cases} P_{\mathrm{R}} = U_{\mathrm{dR}} I_{\mathrm{d}} \\ U_{\mathrm{dR}} - U_{\mathrm{dI}} = I_{\mathrm{d}} R_{\mathrm{d}} \end{cases} \tag{23}$$

Therefore, the apparent power S_{I} delivered by the inverter can be derived as:

$$S_{\mathrm{I}} = \frac{-U_{\mathrm{dI}} + \sqrt{U_{\mathrm{dI}}^2 + 4P_{\mathrm{R}} R_{\mathrm{d}}}}{2R_{\mathrm{d}}} U_{\mathrm{dI}} + \mathrm{j} Q_{\mathrm{I}} \tag{24}$$

From Eq. (24), it can be seen that the variation of the apparent power $\Delta S_{\mathrm{I}} = 0$. Substituting the expressions of S_{I} and ΔS_{I} into (15), the additional equivalent operating admittance of the VSC-HVDC under the control mode can be obtained as:

$$Y_{\Delta m} = \frac{U_{\mathrm{dI}} - \sqrt{U_{\mathrm{dI}}^2 + 4P_{\mathrm{R}} R_{\mathrm{d}}}}{2R_{\mathrm{d}} U_{\mathrm{I}}^2} U_{\mathrm{dI}} + \mathrm{j} \frac{Q_{\mathrm{I}}}{U_{\mathrm{I}}^2} \tag{25}$$

While the rectifier adopts CV control, the inverter adopts CP control and the active power transmitted is P_{I}. Similarly, the additional equivalent operating admittance of the VSC-HVDC under the control mode can be obtained as:

$$Y_{\Delta m} = -\frac{P_{\mathrm{I}}}{U_{\mathrm{I}}^2} + \mathrm{j} \frac{Q_{\mathrm{I}}}{U_{\mathrm{I}}^2} \tag{26}$$

3.2.2 Low Voltage Regulation (LVR) Control

In this control mode, the reactive power Q_{I} delivered by the inverter can be expressed by the bus voltage U_{I}.

$$Q_{\mathrm{I}} = -k_{\mathrm{low}} (U_{\mathrm{I}} - U_{\mathrm{low}}) + Q_0 \tag{27}$$

where k_{low} is the droop coefficient of the low voltage regulation control, and it can be calculated as:

$$k_{\mathrm{low}} = \frac{Q_{\mathrm{max}} - Q_0}{U_{\mathrm{low}} - U_{\mathrm{min}}} \tag{28}$$

While the rectifier adopts CP control and the active power transmitted is P_{R}, the inverter adopts CV control and the DC voltage is U_{dI}. The apparent power S_{I} delivered by the inverter can be derived as:

$$S_{\mathrm{I}} = \frac{-U_{\mathrm{dI}} + \sqrt{U_{\mathrm{dI}}^2 + 4P_{\mathrm{R}} R_{\mathrm{d}}}}{2R_{\mathrm{d}}} U_{\mathrm{dI}} + \mathrm{j} Q_{\mathrm{I}} \tag{29}$$

From Eq. (29), the variation ΔS_{I} of the apparent power can be deduced as:

$$\Delta S_{\mathrm{I}} = -\mathrm{j} k U_{\mathrm{I}} \tag{30}$$

Substituting the expressions of S_{I} and ΔS_{I} into (15), the additional equivalent operating admittance of the VSC-HVDC under the control mode can be obtained as:

$$Y_{\Delta m} = \frac{U_{\mathrm{dI}} - \sqrt{U_{\mathrm{dI}}^2 + 4P_{\mathrm{R}} R_{\mathrm{d}}}}{2R_{\mathrm{d}} U_{\mathrm{I}}^2} U_{\mathrm{dI}} + \mathrm{j} \left(\frac{Q_{\mathrm{I}} + k_{\mathrm{low}} U_{\mathrm{I}}}{U_{\mathrm{I}}^2} \right) \tag{31}$$

While the rectifier adopts CV control and the DC voltage is U_{dR}, the inverter adopts CP control and the active power is P_I. Similarly, the additional equivalent operating admittance of VSC-HVDC under the control mode can be obtained as:

$$Y_{\Delta m} = -\frac{P_I}{U_I^2} + j\left(\frac{Q_I + k_{low}U_I}{U_I^2}\right) \tag{32}$$

3.2.3 High Voltage Regulation (HVR) Control

In this control mode, the additional equivalent operating admittance of VSC-HVDC can be deduced referring to the low voltage regulation control.

While the rectifier adopts CP control and the active power is P_R, the inverter adopts CV control and the DC voltage is U_{dI}. The additional equivalent operating admittance is expressed as:

$$Y_{\Delta m} = \frac{U_{dI} - \sqrt{U_{dI}^2 + 4P_R R_d}}{2R_d U_I^2}U_{dI} + j\left(\frac{Q_I + k_{high}U_I}{U_I^2}\right) \tag{33}$$

While the rectifier adopts CV control, the inverter adopts CP control and the active power is P_I. The additional equivalent operating admittance is expressed as:

$$Y_{\Delta m} = -\frac{P_I}{U_I^2} + j\left(\frac{Q_I + k_{high}U_I}{U_I^2}\right) \tag{34}$$

Observing the additional equivalent operating admittance calculation equations, it can be seen that the additional equivalent operating admittance can be obtained according to the system operating parameters. The additional equivalent operating admittance matrix Y_Δ can be formed.

4 Calculation of HMIIF

In the HMIDC system, the equivalent bus impedance matrix Z_{eq} can be obtained by modifying the original AC system admittance matrix Y with the additional equivalent operating admittance matrix Y_Δ. According to the definition of HMIIF and (12), the calculation expression of the HMIIF between inverter j and i can be obtained as:

$$\text{HMIIF}_{ji} = \frac{\Delta U_j}{\Delta U_i} = \left|\frac{Z_{eqji}I_{0i}}{Z_{eqii}I_{0i}}\right| = \left|\frac{Z_{eqji}}{Z_{eqii}}\right| \tag{35}$$

The complete calculation process of HMIIF is shown in Fig. 4. The proposed calculation method is an improvement of the method based on impedance ratio. The voltage regulation control characteristics of VSC-HVDC are modeled in additional equivalent operating admittance. The control response characteristics of LCC-HVDC and VSC-HVDC are shown by the additional equivalent operating admittance matrix. A more accurate calculation value of HMIIF can be obtained by modifying the impedance of the original power network. It is helpful to evaluate the voltage interaction between the inverters in the HMIDC quickly and accurately.
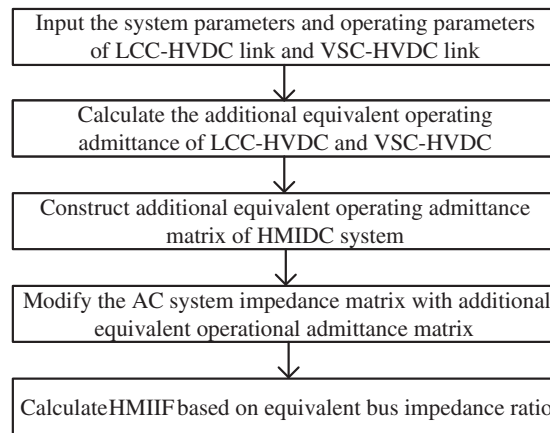
Figure 4: Complete calculation process

5 Case Studies

In order to verify the effectiveness of the HMIIF calculation method, a hybrid dual-infeed HVDC system is built in Power Systems Computer Aided Design (PSCAD). The system structure is shown in Fig. 5. The parameters of CIGRÉ HVDC benchmark system are adopted for LCC-HVDC. The main circuit parameters of VSC-HVDC are shown in Table 1. The inverters of LCC-HVDC and VSC-HVDC are named as inverter 1 and inverter 2, respectively, and the control target values are shown in Table 2. The AC system equivalent impedance parameters are shown in Table 3.
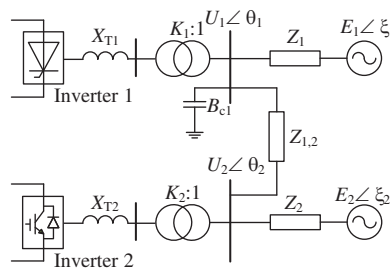
Figure 5: Hybrid dual-infeed system

Table 1: Main circuit parameters of VSC-HVDC link

Parameters	Numerical values
Rated active power	750 MW
Rated DC voltage	± 160 kV
Rated voltage of the converter bus	230 kV
Transformation ratio of transformer	230/175

Table 2: Control target values of different control modes

Types of equipment	Control mode	Target value
LCC-HVDC	CC	2 kA
	CE	18°
VSC-HVDC	CP	750 MW
	CV	160 kV
	CQ	50 MW

Table 3: AC equivalent impedance parameters

Impedance name	Impedance values/Ohms
AC equivalent impedance of LCC	$0.7 + j6.3$
AC equivalent impedance of VSC	$0.9 + j8$
Equivalent coupling impedance	$1.5 + j15$

At 3 s, inverter bus 1 or 2 induces an approximate 1% step voltage through the artificial switched connection of a shunt reactive element and HMIIF is calculated based on the time domain simulation method. In addition, the impedance ratio method and the proposed method are used to calculate HMIIF for comparison.

5.1 Validation of Calculation Method under CQ Control

The AC equivalent source voltage magnitudes of LCC-HVDC and VSC-HVDC are set to 1.05 and 1 pu, respectively. In this case, VSC-HVDC operates in CQ mode. The numerical comparison of different acquisition methods for HMIIF under CQ control mode is shown in Table 4. Since the calculation result deviation of different acquisition methods for HMIIF is small, only the simulation results for calculating $HMIIF_{21}$ are given in Fig. 6. The predicted bus voltage of VSC-HVDC from the impedance ratio method and the proposed method is obtained based on calculated HMIIF, respectively. Similarly, only the simulation results for calculating $HMIIF_{21}$ are given under the LVR control and HVR control.

Table 4: Numerical comparison of different acquisition method for HMIIF

Control mode		$HMIIF_{12}$			$HMIIF_{21}$		
VSC-HVDC		Simulation	Proposed method	Impedance ratio method	Simulation	Proposed method	Impedance ratio method
CQ	CP-CV	0.326919	0.317080	0.312384	0.354695	0.343282	0.348130
CQ	CV-CP	0.325066	0.317092	0.312384	0.350832	0.343139	0.348130

(Continued)

Table 4 (continued)

Control mode		HMIIF$_{12}$			HMIIF$_{21}$		
VSC-HVDC		Simulation	Proposed method	Impedance ratio method	Simulation	Proposed method	Impedance ratio method
LVR	CP-CV	0.328293	0.317347	0.312384	0.283753	0.283225	0.348130
LVR	CV-CP	0.329087	0.317348	0.312384	0.282131	0.283121	0.348130
HVR	CP-CV	0.329230	0.316959	0.312384	0.259004	0.253429	0.348130
HVR	CV-CP	0.329524	0.316959	0.312384	0.256757	0.253400	0.348130

(a) AC voltage   (b) reactive power
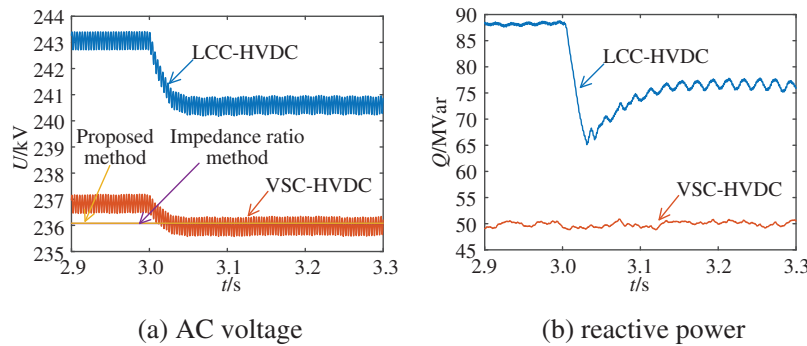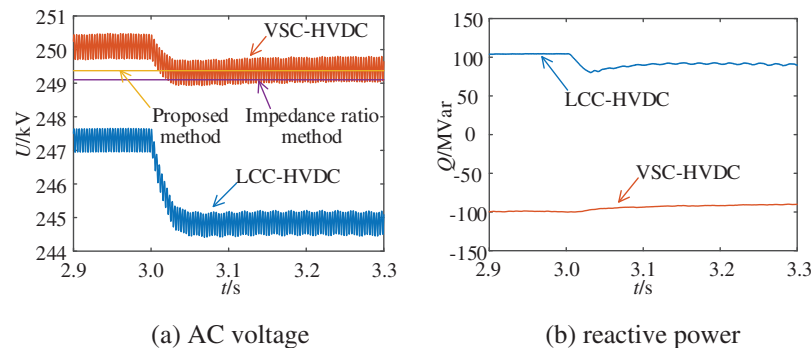
Figure 6: Simulation results under CQ control

Observing the simulation results in Fig. 6, when the bus of LCC-HVDC induces an approximate 1% step voltage under CQ control, the predicted bus voltage of VSC-HVDC from the impedance ratio method and the proposed method is almost the same as the time domain simulation method.

It can be seen from Table 4 that when the VSC-HVDC adopts CQ control, the maximum calculation error of the proposed method is 3.22%, while that of the impedance ratio method is 4.44%. The proposed method considers the control response characteristics of LCC-HVDC and VSC-HVDC. Compared with the impedance ratio method, the proposed method can obtain more accurate index values.

5.2 Validation of Calculation Method under LVR Control

The AC equivalent source voltage magnitudes of LCC and VSC are set to 1.05 and 0.85 pu, respectively. In this case, VSC operates in LVR control mode and the simulation results are shown in Fig. 7. Numerical comparison of different acquisition methods for HMIIF under this control mode is shown in Table 4.

(a) AC voltage   (b) reactive power
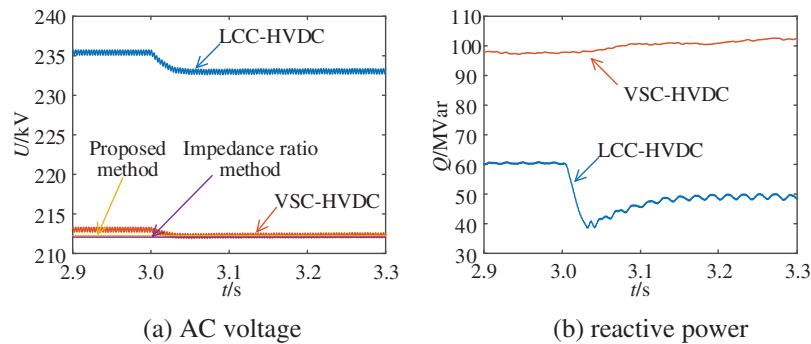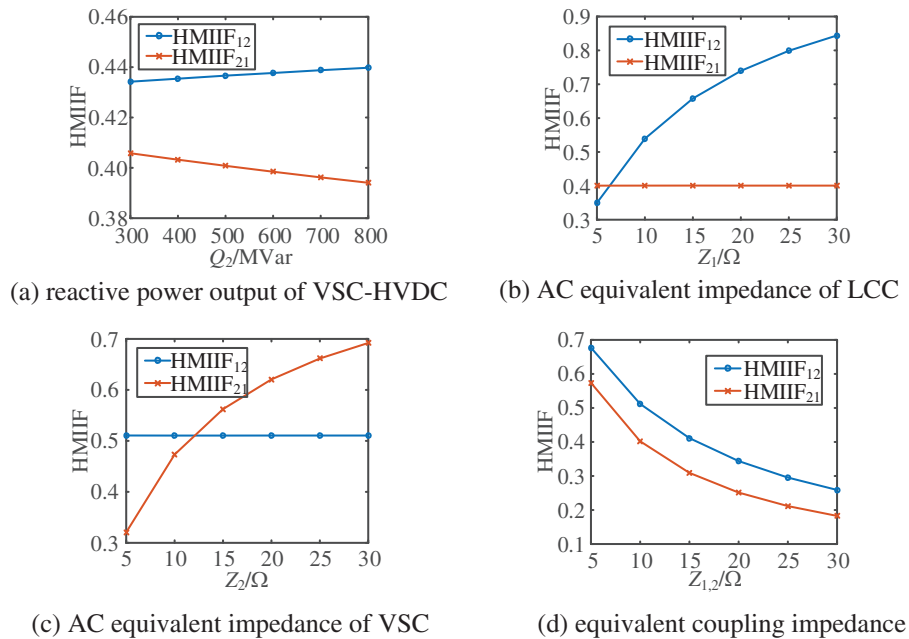
Figure 7: Simulation results under LVR control

Observing the simulation results in Fig. 7, when the bus of LCC-HVDC induces an approximate 1% step voltage under LVR control, the predicted bus voltage of VSC-HVDC from the proposed method is closer to the time domain simulation method than the impedance ratio method.

It can be found from Table 4 that the LVR control of VSC-HVDC nearly has no influence on the $HMIIF_{12}$. It means that the LVR control of VSC-HVDC cannot change the effect of the voltage disturbance at the bus of VSC-HVDC on the bus voltage of LCC-HVDC. However, the HMIIF21 under the LVR control is smaller than that under CQ control. Therefore, the LVR control of VSC-HVDC can weaken the effect of the voltage disturbance at the bus of LCC-HVDC on the bus voltage of VSC-HVDC.

Additionally, Table 4 shows that the maximum calculation error of the proposed method is 3.56%, while that of the impedance ratio method is 5.07%. The proposed method considers the LVR control characteristics of VSC-HVDC. Compared with the impedance ratio method, the calculation error is smaller.

5.3 Validation of Calculation Method under HVR Control

The AC equivalent source voltage magnitudes of LCC and VSC are set to 1.05 and 1.1 pu, respectively, and the voltage phase angles are both set to 0. In this case, VSC operates in HVR control mode and the simulation results are shown in Fig. 8. Numerical comparison of different acquisition methods for HMIIF under this control mode is shown in Table 4.

(a) AC voltage   (b) reactive power

Figure 8: Simulation results under HVR control

Observing the simulation results in Fig. 8, when the bus of LCC-HVDC induces an approximate 1% step voltage under HVR control, the predicted bus voltage of VSC-HVDC from the proposed method is closer to the time domain simulation method than the impedance ratio method.

From Table 4, the HVR control of VSC-HVDC cannot change the effect of the voltage disturbance at the bus of VSC-HVDC on the bus voltage of LCC-HVDC. However, the HVR control of VSC-HVDC can weaken the effect of the voltage disturbance at the bus of LCC-HVDC on the bus voltage of VSC-HVDC. It can be seen the $HMIIF_{21}$ under the HVR control is smaller than that under the LVR control. The reason for the phenomenon is that there is a bigger droop coefficient in the HVR control mode.

Moreover, it can be found in Table 4 that the maximum calculation error of the proposed method is 3.81%, while that of the impedance ratio method is 5.20%. The proposed method considers voltage regulation control characteristics of VSC-HVDC. Compared with the impedance ratio method, the calculation accuracy is higher.

5.4 The Influence of Reactive Power from VSC-HVDC on HMIIF

In the HMIDC system, changing reactive power from VSC-HVDC can alter the DC additional equivalent operating admittance, thereby affecting the HMIIF index. Adjust the reactive power target value of VSC-HVDC to obtain the HMIIF as shown in Fig. 9a.

(a) reactive power output of VSC-HVDC

(b) AC equivalent impedance of LCC

(c) AC equivalent impedance of VSC

(d) equivalent coupling impedance

Figure 9: Influence of reactive power from VSC-HVDC and AC system impedance on HMIIF

Observing Fig. 9a, it can be seen that as the reactive power from VSC-HVDC increases, the $HMIIF_{12}$ increases, indicating that the voltage disturbance of VSC-HVDC converter bus has a greater impact on the voltage of other converter buses, while the $HMIIF_{21}$ decreases, indicating that the voltage disturbance of other converter buses has a smaller impact on the voltage of VSC-HVDC converter bus. Therefore, when voltage disturbances occur at the VSC-HVDC converter bus, the reactive power from VSC-HVDC should be appropriately reduced. When voltage disturbances occur at other converter

buses, increasing the reactive power output of VSC-HVDC appropriately can reduce the interaction between converter bus voltages, which is beneficial for maintaining the voltage stability of other converter buses.

5.5 *The Influence of AC System Equivalent Impedance on HMIIF*

For a simplified model of a hybrid multi-infeed AC/DC system, the equivalent impedance of the AC system includes the equivalent source impedance and the equivalent coupling impedance, whose values directly determine the node impedance of the AC system, thereby affecting the HMIIF. By simply changing the AC equivalent impedance Z_1 of LCC-HVDC, the AC equivalent impedance Z_2 of VSC-HVDC, and the equivalent coupling impedance $Z_{1,2}$, the HMIIF index is shown in Fig. 9.

From Figs. 9b and 9c, it can be seen that as the AC equivalent impedance of LCC increases, $HMIIF_{12}$ increases, while $HMIIF_{21}$ remains almost unchanged. As the AC equivalent impedance of VSC increases, $HMIIF_{21}$ increases, while $HMIIF_{12}$ remains almost unchanged. Observing Fig. 9d, an increase in equivalent coupling impedance can simultaneously reduce $HMIIF_{12}$ and $HMIIF_{21}$ weakening the voltage interaction between the converters.

6 Discussion

Based on the above case study, different control modes, reactive power from VSC-HVDC, and AC system equivalent impedance will affect HMIIF. The main findings are as follows:

1) The voltage regulation control of VSC-HVDC greatly affects the $HMIIF_{21}$ but nearly has no influence on the $HMIIF_{12}$. The voltage regulation control of VSC-HVDC can reduce the $HMIIF_{21}$. It means that the voltage regulation control can weaken the effect of the voltage disturbance at the bus of LCC-HVDC on the bus voltage of VSC-HVDC, which can help to maintain the voltage stability of the power grid.

2) The increase in the reactive power from VSC-HVDC can decrease the $HMIIF_{21}$. When voltage disturbances occur, increasing the reactive power from VSC-HVDC appropriately can reduce the interaction between converter bus voltages, which is beneficial for maintaining the voltage stability of other converter buses.

3) The increase in the AC equivalent impedance of LCC-HVDC can increase $HMIIF_{12}$, and the increase in the AC equivalent impedance of VSC-HVDC can increase $HMIIF_{21}$. Decreasing AC equivalent impedance can reduce the influence on the converter bus voltage from the voltage disturbances occurring at other converter buses. The increase in equivalent coupling impedance can simultaneously reduce $HMIIF_{12}$ and $HMIIF_{21}$, weakening the voltage interaction between the converters.

7 Conclusion

In this paper, a hybrid multi-infeed interaction factor calculation method considering voltage regulation control characteristics of VSC-HVDC is proposed, and a hybrid dual-infeed DC system is constructed for simulation verification and analysis. The calculation method based on the equivalent bus impedance ratio can be used to obtain HMIIF. Only relying on the operating parameters and the AC system admittance matrix, the HMIIF between inverters can be calculated at one time with fast calculation speed and high accuracy. And the HMIIF under different control modes are greatly different. It cannot be ignored the influence of the control mode while analyzing the voltage interaction between inverters. The voltage regulation control of VSC-HVDC can weaken the effect of the voltage

disturbance at the bus of LCC-HVDC on the bus voltage of VSC-HVDC, which can help to maintain the voltage stability of the power grid.

Author Contributions: The authors confirm contribution to the paper as follows: Study conception and design: Tuo Wang; data collection: Fengze Han, Tuo Wang; analysis and interpretation of results: Shan Liu, Chengbin Chi, Yanan Wu, Lin Zhu; draft manuscript preparation: Fengze Han, Tuo Wang. All authors reviewed the results and approved the final version of the manuscript.

Availability of Data and Materials: All data generated or analysed during this study are included in this published article.

Conflicts of Interest: The authors declare that they have no conflicts of interest to report regarding the present study.

References

1. C. Wu, D. Zhang, and J. He, "A double-ended protection principle for an LCC-VSC-MTDC system with strong anti-interference ability," *Energy Eng.*, vol. 120, no. 2, pp. 299–316, Nov. 2022. doi: 10.32604/ee.2023.023532.

2. D. Zhang, C. Wu, and J. He, "Single-ended protection principle for LCC-VSC-MTDC system with high resistance fault tolerance," *Energy Eng.*, vol. 120, no. 1, pp. 1–21, Oct. 2022. doi: 10.32604/ee.2022.023304.

3. H. Xiao, X. Duan, Y. Zhang, and Y. Li, "Comparative analysis of inter-inverter interactions in emerging hierarchical-infeed and conventional multi-infeed LCC-HVDC systems," *IEEE Trans. Energy Convers.*, vol. 38, no. 1, pp. 27–37, Mar. 2023. doi: 10.1109/TEC.2022.3192489.

4. M. Szechtman, M. J. Ximenes, and A. R. Saavedra, "Comparative analysis of stability and electromagnetic transient studies for HVDC multi-infeed systems," *CSEE J. Power Energy Syst.*, vol. 3, no. 3, pp. 253–259, Sep. 2017. doi: 10.17775/CSEEJPES.2016.01730.

5. R. Shah, J. C. Sánchez, R. Preece, and M. Barnes, "Stability and control of mixed AC-DC systems with VSC-HVDC: A review," *IET Gener. Transmiss. Distrib.*, vol. 12, no. 10, pp. 2207–2219, Apr. 2018. doi: 10.1049/iet-gtd.2017.1140.

6. I. E. Maysse *et al.*, "Nonlinear observer-based controller design for VSC-based HVDC transmission systems under uncertainties," *IEEE Access*, vol. 11, pp. 124014–124030, Nov. 2023. doi: 10.1109/ACCESS.2023.3330440.

7. I. E. Maysse *et al.*, "Observer and nonlinear control design of VSC-HVDC transmission system," *Int. J. Electr. Power Energy Syst.*, vol. 145, pp. 108609, Feb. 2023. doi: 10.1016/j.ijepes.2022.108609.

8. D. Oliveira, G. C. B. Leal, D. Herrera, E. Galván-Díez, J. M. Carrasco and M. Aredes, "An analysis on the VSC-HVDC contribution for the static voltage stability margin and effective short circuit ratio enhancement in hybrid multi-infeed HVDC systems," *Energies*, vol. 16, no. 1, pp. 532, doi: 10.3390/en16010532.

9. H. Xiao and Y. Li, "Multi-infeed voltage interaction factor: A unified measure of inter-inverter interactions in hybrid multi-infeed HVDC systems," *IEEE Trans. Power Del.*, vol. 35, no. 4, pp. 2040–2048, Dec. 2019. doi: 10.1109/TPWRD.2019.2960393.

10. H. H. Yin *et al.*, "Interaction mechanism analysis and additional damping control for hybrid multi-infeed HVDC system," *IEEE Trans. Power Del.*, vol. 37, no. 5, pp. 3904–3916, Oct. 2022. doi: 10.1109/TP-WRD.2022.3140826.

11. CIGRE Working Group B4.41, "Systems with multiple DC infeed," *Technical Brochure 364*, Paris, France: CIGRE, 2008, pp. 16–19.

12. Y. Shao and Y. Tang, "Fast evaluation of commutation failure risk in multi-infeed HVDC systems," *IEEE Trans. Power Syst.*, vol. 33, no. 1, pp. 646–653, May 2017. doi: 10.1109/TPWRS.2017.2700045.

13. H. Xiao, H. Li, A. M. Gole, and X. Duan, "Computationally efficient and accurate approach for commutation failure risk areas identification in multi-infeed LCC-HVdc systems," *IEEE Trans. Power Electron*, vol. 35, no. 5, pp. 5238–5253, Sep. 2019. doi: 10.1109/TPEL.2019.2943182.

14. X. Chen, A. M. Gole, and M. Han, "Analysis of mixed inverter/rectifier multi-infeed HVDC systems," *IEEE Tran. Power Del.*, vol. 27, no. 3, pp. 1565–1573, Mar. 2012. doi: 10.1109/TPWRD.2012.2187356.

15. D. L. H. Aik and G. Andersson, "Analysis of voltage and power interactions in multi-infeed HVDC systems," *IEEE Trans. Power Del.*, vol. 28, no. 2, pp. 816–824, Jan. 2013. doi: 10.1109/TPWRD.2012.2227510.

16. C. Xia, X. Hua, Z. Wang, and Z. Huang, "Analytical calculation for multi-infeed interaction factors considering control modes of high voltage direct current links," *Energies*, vol. 11, no. 6, pp. 1506, doi: 10.3390/en11061506.

17. F. Zhang *et al.*, "Study on calculation method of multi-infeed HVDC interaction factor considering small disturbance response characteristics of HVDC transmission system," (in Chinese), *Proc. CSEE*, vol. 39, no. 18, pp. 5308–5315, Sep. 2019.

18. Q. Guo, M. Yoon, C. Kim, and G. Jang, "Commutation failure and voltage sensitivity analysis in a hybrid multi-infeed HVDC system containing modular multilevel converter," *Int. Trans. Elect. Energy Syst.*, vol. 26, no. 10, pp. 2259–2271, Oct. 2016. doi: 10.1002/etep.2206.

19. C. Guo, W. Liu, C. Zhao, and X. Ni, "Small-signal dynamics and control parameters optimization of hybrid multi-infeed HVDC system," *Int. J. Electr. Power Energy Syst.*, vol. 98, pp. 409–418, Jun. 2018. doi: 10.1016/j.ijepes.2017.12.009.

20. C. Guo, W. Liu, J. Zhao, and C. Zhao, "Impact of control system on small-signal stability of hybrid multi-infeed HVDC system," *IET Gener. Transmiss. Distrib.*, vol. 12, no. 19, pp. 4233–4239, Oct. 2018. doi: 10.1049/iet-gtd.2018.5087.

21. Q. Li, T. Wang, C. Mao, Z. Li, Y. Xin and S. Jiang, "Multi-infeed interaction factor calculation method of hybrid multi-infeed HVDC system considering DC control characteristics," (in Chinese), *Power Syst. Tech.*, vol. 45, no. 8, pp. 3125–3133, Aug. 2021.

22. D. Liu, D. Shi, and Y. Li, "A new definition of short-circuit ratio for multi-converter HVDC systems," *J. Electr. Eng. Tech.*, vol. 10, no. 5, pp. 1958–1968, Sep. 2015. doi: 10.5370/JEET.2015.10.5.1958.

23. B. Rehman, C. Liu, H. Li, C. Fu, and W. Wei, "Analysis on local and concurrent commutation failure of multi-infeed HVDC considering inter-converter interaction," *J. Modern Power Syst. Clean Energy*, vol. 10, no. 4, pp. 1050–1059, Jun. 2021. doi: 10.35833/MPCE.2020.000164.

24. W. Yao, L. Wang, H. Zhou, Y. Xiong, and J. Wen, "Harmonics interaction mechanism and impact on extinction angles in multi-infeed HVDC systems," *IEEE Trans. Power Del*, vol. 38, no. 4, pp. 2427–2440, Feb. 2023. doi: 10.1109/TPWRD.2023.3243412.